

Morphological Analysis of CEERS MIRI pointings in comparison to 3D-HST AEGIS field.

B. Rajpoot^{1,*} and L. Boogaard (Supervisor)^{2,†}

¹*Department of Physics and Astronomy, Universität Heidelberg, 69117 Heidelberg, Germany*

²*Max Planck Institute for Astronomy, D-69117 Heidelberg, Germany*

This project aimed to perform a morphological analysis of the James Webb Space Telescope's Mid-Infrared Instrument (JWST's MIRI) imaging data of the pointings from the CEERS survey. We used the F560W imaging data from the CEERS DR0.5 of MIRI 6 pointing, whose results were later compared with the F160W imaging of the 3D-HST catalog.

From our analysis, we detected 169 sources crossmatched with the 3D-HST catalog, out of which 89 galaxies were identified to be at the cosmic noon ($z \sim 1-3$). These galaxies showed a decreasing trend of the apparent magnitude with respect to redshift. The magnitude comparison of the detected sources at F560W vs F160W and IRAC3 followed mainly a 1:1 trend with a few outliers. We further detected an astrometric shift of (0.11,-0.2) arcsec in the crossmatched sources with so far unknown origin. From the successful morphology fitting of 62 galaxies, we report the majority of the fitted galaxies had a half-light radius of less than 1'' with an average Sérsic Index of less than 5. We also report the detection of two galaxies in the MIRI F560W, which were undetected in HST F160W, indicating the possibility of high-redshift Lyman-break galaxies in the field. This project proved crucial in increasing the understanding of the reduction and analysis process of the JWST data along with the importance of studying and probing the galactic evolution of the galaxies at the cosmic noon in the Mid-Infrared regime.

Keywords: galaxies: photometry; methods: data analysis; techniques: image processing; Astrophysics - Cosmology and Extragalactic Astrophysics

| | | |
|--|--|----|
| CONTENTS | Acknowledgments | 10 |
| I. Introduction | | |
| II. Data | | |
| III. Analysis | | |
| A. Source-Extraction with SEP | | |
| 1. MAST Files | 2 | |
| 2. Challenges with MAST files | 2 | |
| 3. DR0.5 files | 3 | |
| 4. Flux Conversions | 4 | |
| 5. Running <i>SEP</i> in Dual-Image mode | 6 | |
| B. Catalog Matching | 6 | |
| C. Morphology Fitting | 6 | |
| IV. Results | | |
| V. Discussions & Conclusion | | |
| VI. Future Prospects | | |
| | VII. Appendix | 10 |
| | A. Code for creating Erosion Mask for MAST files | 10 |
| | B. Code snippet for generating a table of the extracted sources on CEERS MIRI DR0.5 fits files. | 12 |
| | C. <i>PetroFit</i> plots at different redshifts | 12 |
| | References | 13 |
| | I. INTRODUCTION | |
| | The size evolution of galaxies throughout different redshifts can tell us critical information about the potential formation and evolution scenarios undergone by the early high-redshift galaxies, especially during the Cosmic Noon at $z \sim 1-3$, when nearly all the galaxies in the universe went into intense star formation (Madau and Dickinson 2014, van der Wel et al. 2014). Due to the redshift range, the most ideal wavelength to study the size evolution is in the Mid- | 7 |

* bhavesh.rajpoot@stud.uni-heidelberg.de

† boogaard@mpia.de

Infrared Range.

Since its launch, JWST has provided a unique window on Galaxies in the Mid & Near-Infrared ranges. With 7 times more gathering power than the Hubble Space Telescope (HST), the increased resolving power and the limiting magnitude in the Infrared regime allows us to see more resolved details. This presents us with the opportunity to study and compare the morphology of the galaxies to study dust-obscured star formation in the galaxies at the peak cosmic star formation time at $z \sim 1\text{-}3$ (Kartaltepe et al. 2023, Suess et al. 2022).

For this purpose, we use The Cosmic Evolution Early Release Science Survey (CEERS) project (PID 1345) (Finkelstein et al. 2022, 2017), which aims to demonstrate, test, and validate efficient extragalactic surveys with coordinated, overlapping parallel observations with the JWST instrument suite by providing imaging and spectroscopy of the Extra-Galactic Survey (EGS) HST legacy field with six parallel JWST instrument modes.

We primarily focus on analysing the broadband imaging at $5.6\ \mu\text{m}$ with JWST's MIRI at the CEERS no. 6 pointing from the June Configuration. We aimed to compare the sizes of the galaxies detected in MIRI images at $5.6\ \mu\text{m}$ to the sizes previously measured by the 3D-HST catalog (Brammer et al. 2012, Momcheva et al. 2016, Skelton et al. 2014) at $1.6\ \mu\text{m}$ (Kartaltepe et al. 2023, Suess et al. 2022).

II. DATA

As the CEERS data is open to the public, one can easily download the data products from the STScI's Barbara A. Mikulski Archive for Space Telescopes (MAST) portal. We use the Resampled 2D data (`.i2d`) files which is a Stage 3 data product from JWST Science Calibration Pipeline.

Each `.i2d` file is a multi-extension header file, as shown in the table I, where the `SCI` ext. contains 2D data array of the pixel values, in units of surface brightness (MJy/sr) and `ERR` ext. contains resampled uncertainty estimates, given as standard deviation. More details are available

on the [JWST pipeline website](#).

During the later stages of the project, we used the CEERS preliminary [DR0.5 release](#) for our analysis. The survey planned in total eight MIRI pointings in the AEGIS field, out of which we analysed the 6th pointing which was observed in June 2022 with a depth of 26.2 ABMag at 5σ pt. source.

III. ANALYSIS

A. Source-Extraction with SEP

The first step of mainly every photometrical analysis is detecting all the sources in the image and performing their Aperture Photometry. For this task, we use the Python library for Source-Extractor and Photometry (`SEP`) by Barbary (2016), which is based on the original Source-Extractor code by Bertin and Arnouts (1996). Source-Extractor is a program that builds a catalog of objects from an astronomical image.

1. MAST Files

The `.i2d` files produced by the [JWST Pipeline](#) are resampled but without background subtraction which is required to perform source extraction. `SEP` provides an in-built functionality to perform this and can be accessed through `sep.background()` command. So, the basic workflow to analyse the images becomes:

- : Background Subtraction [`sep.background()`]
- : Object detection [`sep.extract()`]
- : Aperture Photometry [`sep.sum_ellipse()`]

For the source extraction, we used a modified configuration inspired by Hot & Cold Modes (Table 2 in Galametz et al. 2013, page 7) for effective source detection in MIRI images. The parameter values used are listed in the table II.

2. Challenges with MAST files

On further probing the data, we found out that the images had an astrometric offset, due

| No. | Name | Ver | Type | Cards | Dimensions | Format |
|-----|-------------|-----|-------------|-------|--------------|----------------|
| 0 | PRIMARY | 1 | PrimaryHDU | 338 | N/A | N/A |
| 1 | SCI | 1 | ImageHDU | 75 | (1036, 1034) | float32 |
| 2 | ERR | 1 | ImageHDU | 10 | (1036, 1034) | float32 |
| 3 | CON | 1 | ImageHDU | 9 | (1036, 1034) | int32 |
| 4 | WHT | 1 | ImageHDU | 9 | (1036, 1034) | float32 |
| 5 | VAR_POISSON | 1 | ImageHDU | 9 | (1036, 1034) | float32 |
| 6 | VAR_RNOISE | 1 | ImageHDU | 9 | (1036, 1034) | float32 |
| 7 | VAR_FLAT | 1 | ImageHDU | 9 | (1036, 1034) | float32 |
| 8 | HDRTAB | 1 | BinTableHDU | 816 | 3R x 403C | [23A, 5A, ...] |

Table I: The FITS file structure of a RAW .i2d file

| Parameter Names | | Values |
|-----------------|-----------------|---|
| sep | SExtractor | |
| thresh | DETECT_THRESH | 1.5 |
| err | | $(\text{bkg.globalrms}^2 + \text{ERR}^2)^{0.5}$ |
| minarea | DETECT_MINAREA | 3 |
| filter_kernel | FILTER_NAME | Gauss_4.0_7x7.conv |
| filter_type | FILTER | conv |
| deblend_nthresh | DEBLEND_NTHRESH | 48 |
| deblend_cont | DEBLEND_MINCONT | 0.0008 |
| clean | CLEAN | True |
| clean_param | CLEAN_PARAM | 1.0 |
| fw & fh | BACK_SIZE | 32 |
| bw & bh | BACK_FILTERSIZE | 3 |

Table II: Parameter configuration used in SEP for analysis MAST files

to which a lot of artifacts were introduced at the edges (fig. 1). The first half of the project was dedicated to the successful analysis of these MAST files by properly removing the false detections and artifacts.

One of the solutions to overcome this challenge was to re-run the JWST Calibration Pipeline again on the images to perform background subtraction and generate a precise error map. Although, due to the limited working hours and high technicality of the pipeline, we decided to manually remove artifacts at the edges by creating a boolean erosion mask using `skimage.morphology.binary_erosion`. The snippet for the process is listed in the appendix, VII A.

3. DR0.5 files

With the release of CEERS DR0.5 in November, 2022, Yang et al (in prep.), the challenges with the MAST files were solved as the data release provided,

- fully reduced mosaics
- astrometrically registered to the existing HST/CANDELS v1.9 WFC3 and ACS images. (Yang et al. (in prep))
- custom-produced RMS maps, which accounts for poisson, readout, and correlated pixel noise, using `astroRMS` package based on SCI & WHT images
- Pixel scale = 0.09 arcsec/pixel; AB Zero-point = 25.7 mag

The DR0.5 data products didn't require any additional background subtraction or erosion

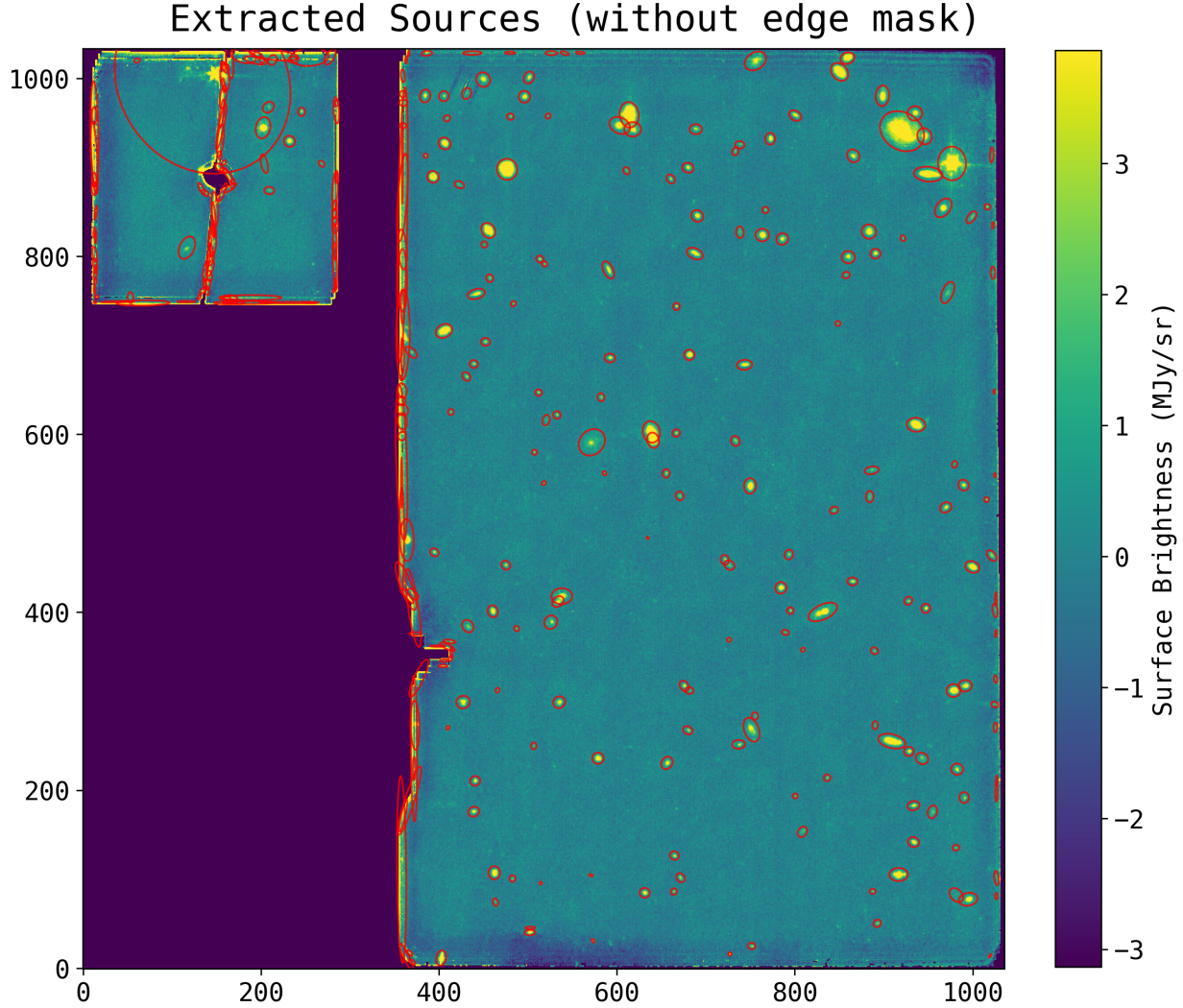


Figure 1: Plot of all the detected sources by SEP without using the boolean binary erosion mask on the MAST image of MIRI6 pointing.

mask. Due to the custom RMS map, there were no false detections or artifacts. This improved the extraction process by several folds, fig. 2. The workflow for analysing these images becomes,

- : Object detection [`sep.extract()`]
- : Aperture Photometry [`sep.sum_ellipse()`]

4. Flux Conversions

The MIRI images are calibrated in the units of Flux Densities, MJy/sr. In order to perform aperture photometry using `sep.sum_ellipse()`,

which sums over pixels, we need to take into account the conversion to Jy/pixel. Therefore, it is required to convert the input fluxes from MJy/sr to Jy/pixel, so that we get fluxes in Jy as an output. After that, the fluxes were converted back into ABMag, in which fluxes are usually reported in catalogs, for easier comparisons of the results across catalogs. To make this whole process more streamlined, we implement this whole process of conversion by modifying the original formula of ABMag, such that it takes input fluxes in MJy/sr and outputs fluxes in ABMag.

The SCI header of MIRI images has all the required information, as reported in table III, needed to perform the conversions.

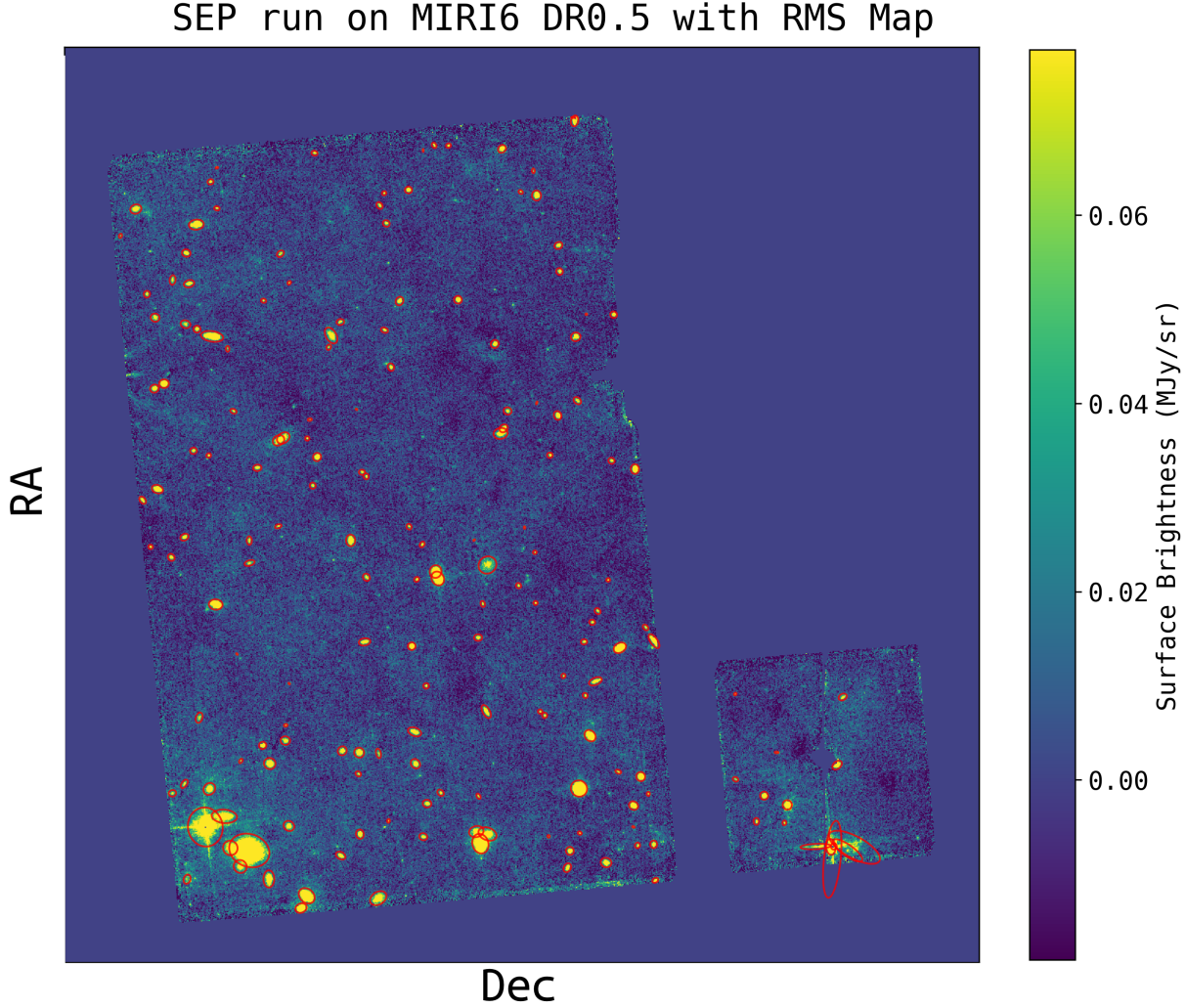


Figure 2: Plot of all the detected sources by **SEP** on DR0.5 image of MIRI6 pointing.

| Name | Value |
|----------|--------------------------------|
| PHOTMJSR | 0.579 MJy/sr |
| PHOTUJA2 | 13.617 uJy/arcsec ² |
| PIXAR_SR | 2.844e-13 sr |
| PIXAR_A2 | 0.0121 arcsec ² |

Table III: List of HEADER keywords in CEERS MIRI images which were used in performing flux conversions. The first two stand for flux densities producing 1 cps (counts per second), and the later two stand for nominal pixel area.

The derivation of the modified ABMag formula goes as follows:

According to the definition of ABMag (Absolute Magnitude), the logarithm of a spectral flux

density (f_ν) with the usual scaling of astronomical magnitudes and a zero-point (ZP) of 3631 Jy, we can write:

$$m_{AB} = -2.5 \log f_\nu + ZP = -2.5 \log \left(\frac{f_\nu}{3631 Jy} \right) \quad (1)$$

As `sep.sum_ellipse` performs sum over pixels enclosed in the ellipse, therefore:

$$F_\nu [\text{MJy}] = \sum_{pixels} f_{\text{MJy/pix}} \quad (2)$$

$$= \sum_{pixels} f_{\text{MJy/sr}} \cdot \left(\frac{sr}{pix} \right) \quad (3)$$

$$= \left(\frac{sr}{pix} \right) \cdot \sum_{pixels} f_{\text{MJy/sr}} \quad (4)$$

(5)

where,

- $pixels$ = no. of pixels enclosed in the ellipse
- sr/pix = pixel area in steradians
- $f_{\text{MJy/sr}}$ = flux density of each individual pixel in MJy/sr
- F_ν = total integrated flux inside the ellipse

Substituting F_ν from 2 to 1, we get:

$$m_{AB} = -2.5 \log \left(\frac{F_\nu}{3631 J_y} \right) \quad (6)$$

$$= -2.5 \log \left(\frac{\left(\frac{sr}{pix} \right) \cdot \sum_{pixels} f_{\text{MJy/sr}}}{3631 J_y} \right) \quad (7)$$

solving this by separating all the constants from the flux density would result in,

$$m_{AB} = -2.5 \log (\sum_{pixels} f_{\text{MJy/sr}}) + ZP' \quad (8)$$

where,

$$ZP' = -2.5 \log \left[\left(\frac{sr}{pix} \right) \times \frac{1e6}{3631} \right] \quad (9)$$

$$= -2.5 \log \left[\left(\frac{[\text{pixel scale}] \cdot \pi}{180} \right)^2 \times \frac{1e6}{3631} \right] \quad (10)$$

To propagate RMS errors (f_{ν_err}) from MJy/sr to ABMag, we perform error propagation as stated in eq. 11.

$$m_{AB_err} = \frac{2.5}{\log 10} \cdot \frac{f_{\nu_err}}{f_\nu} \quad (11)$$

Note, if the physical units of the image are in uJy/arcsec², then the formula for calculating ZP' becomes:

$$ZP' = -2.5 \log \left[\frac{([\text{pixel scale}] \cdot 3600)^2}{3631e6} \right] \quad (12)$$

5. Running SEP in Dual-Image mode

As SEP is built upon the original Source-Extractor code, therefore, it also supports the Dual-Image mode for analysing a pointing's observations in several filters.

Because SEP makes the core algorithms available as a library of stand-alone functions and classes, therefore, they operate directly on in-memory arrays so the Dual-Image mode is not available as a stand-alone function or class.

Algorithm for the Dual-Image mode:

- S1.:** Run SEP on one filter image, ex. on F560W `sep.extract(img_F560W)`, and generate the catalog.
- S2.:** Perform photometry on F560W catalog objects.
- S3.:** Take the next filter image, ex. F770W, and perform photometry, but by using the positional data from the F560W catalog.

The `sep.extract()` function at the Object Detection step outputs a catalog in the format of an AstroPy table, whereas the Aperture Photometry tests enrich the table with photometric information such as summed over flux of a detected source, Kron radius, etc.

B. Catalog Matching

We then perform cross-matching with the 3D-HST AEGIS catalog to compare the properties of the detected sources, such as their Flux, Kron Radius, etc., with the matched detections in the 3D-HST AEGIS catalog. For this, we used the following steps:

- Reading the reference catalog in AstroPy table format

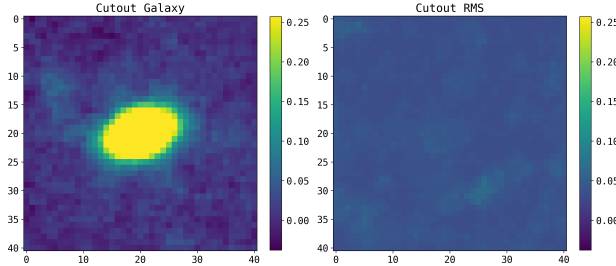


Figure 3: Plot of the cutout stamp of $3.6'' \times 3.6''$ of the galaxy and it's RMS map.

- Using WCS to convert the `(ra,dec)` of detected sources by SEP from pix to degrees.
- Taking the source coordinate values in both the catalogs and making them an AstroPy celestial coordinate object by using `astropy.coordinates.SkyCoord`.
- Using `search_around_sky` on the ref. catalog's coordinate object to perform the cross-match distance threshold of ~ 0.6 arcsecs.
- Exporting the tables of matched sources.

C. Morphology Fitting

We then fit different morphological models to the individual detected galaxies in order to estimate their size and morphology, fig. 3.

We used `PetroFit` by Geda et al. (2022), a Python-based package for estimating the Petrosian properties of galaxies. As `PetroFit` works in the AstroPy environment, therefore, it allows us to pass with Numpy arrays.

The algorithm to perform the fitting is to begin with defining a 2D Sérsic model by using `astropy.modeling.models.Sérsic2D()` and convolve it with the normalized PSF by using `petrofit.modeling.PSFConvolvedModel2D()`. Then fitting the convolved model on the cutout image by using `petrofit.modeling.fit_model()`.

One can visualise the model and residuals plot by using `petrofit.modeling.plot_fit()`, fig. 4.

We select the galaxies only at the cosmic noon

for morphological fitting. The 2D Sérsic model was provided with the parameters from the SEP catalog for each galaxy.

IV. RESULTS

In the MIRI 6 pointing, we detected 177 sources in total, out of which 169 sources were crossmatched successfully with the AEGIS catalog. Out of those remaining 8, 6 were false detections, and 2 were classified as undetected sources in the AEGIS.

From the morphological fitting step, we got successful fits for 62 galaxies out of 89 cosmic noon galaxies. From these 62 galaxies, 7 galaxies showed hidden spiral structures after fitting, and 5 galaxies accounted as outliers.

In fig. 5, we plot the Magnitude distribution of the sources detected in the MIRI field, which resembles a Poissonian distribution. To further investigate the magnitudes, we plot a comparison between MIRI F560W magnitudes and 3D-HST F160W & IRAC3 ($5.8 \mu\text{m}$) fluxes, fig. 6.

In fig. 7, we report the distribution of detected galaxies with respect to their reported redshift in the 3D-HST catalog.

Taking results from the morphological fitting, we plot the derived half-light radius with respect to the redshift of the galaxies at cosmic noon in fig. 9. The marker color represents the derived Sérsic Index from `PetroFit`.

Fig. 8 shows the size comparison of the detected sources, and fig. 10 shows the astrometric offset discovered during the analysis. Fig. 11 shows the cutout of the undetected source in both MIRI and HST images.

V. DISCUSSIONS & CONCLUSION

The distribution's peak in fig. 5 is approximately 1.5 magnitudes brighter than the reported depth of 26.2 ABMag, which follows in agreement with the extraction threshold we had set in SEP. The brighter threshold was chosen primarily for selecting the sources which are bright and big enough to get the morphology done.

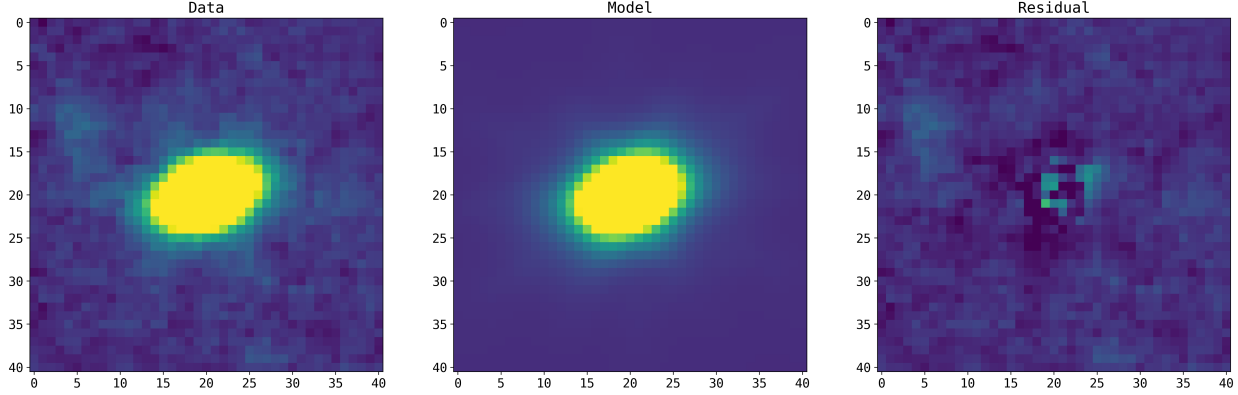


Figure 4: Results from PetroFit. The middle stamp shows the PSF-convolved 2D Sérsic model fitted over the galaxy in the leftmost stamp. And in the rightmost stamp, we have the residuals from the fitted model.

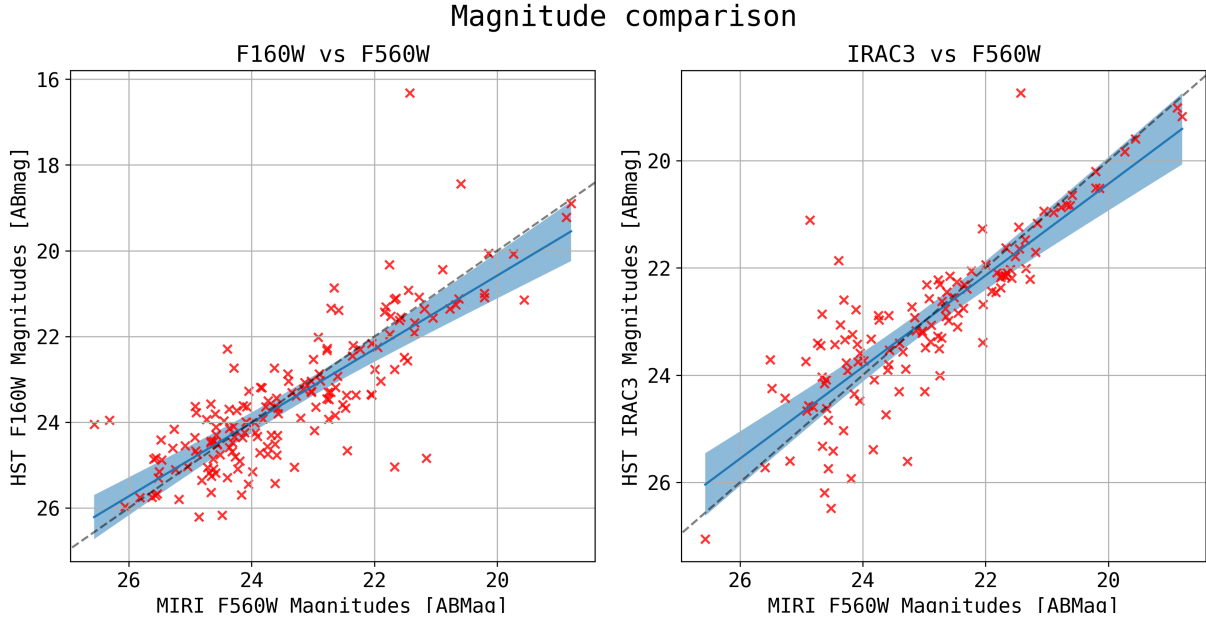


Figure 5: Comparison plot of the magnitudes of detected sources in (a) F160W vs F560W and (b) IRAC3 vs F560W.

Fig. 5 shows the trend between the reported flux in the HST F160W filter & Spitzer IRAC3 channel and the calculated flux in the MIRI F560W filter. The trend is linear and is almost 1:1, with outliers deviating the fit from the exact 1:1 trend. This shows that our results are in agreement with what has been reported before, which also confirms that the flux calibration and aperture photometry was successful too. The outliers in fig. 5 (a) hints towards higher precision of MIRI and the outliers in fig. 5 (b) hints

towards the Heteroscedastic nature of the data due to higher uncertainty in accurate flux determination of the faint sources.

Fig. 7 shows 169 galaxies detected at the Cosmic Noon, $z \sim 1\text{--}3$. These galaxies can serve as good candidates to understand the rate of growth and evolution during Cosmic Noon. There are higher redshift sources too that can be used to compare the morphology results with the candidates in the cosmic noon.

We also performed a crude analysis of the

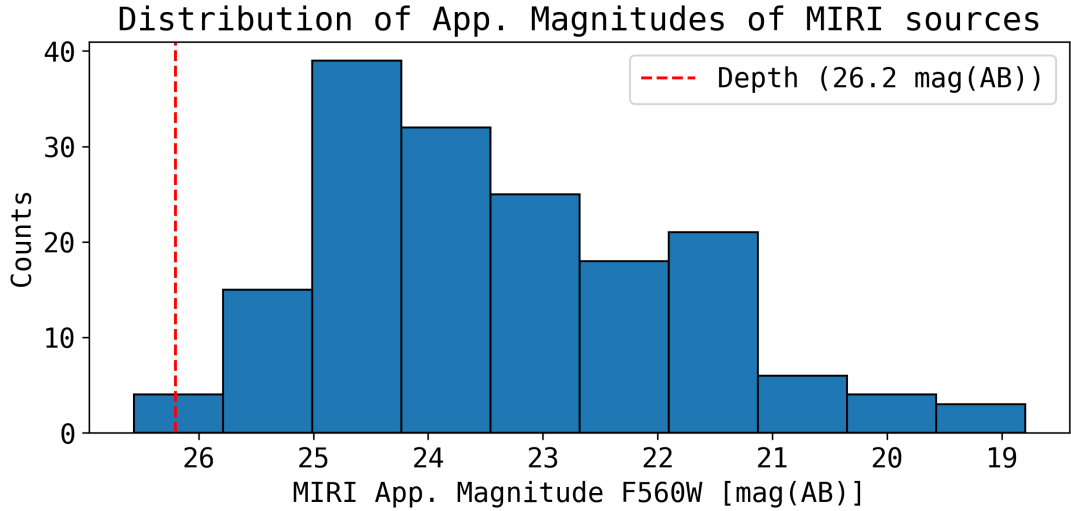


Figure 6: Distribution of MIRI apparent magnitudes of the SEP detected sources

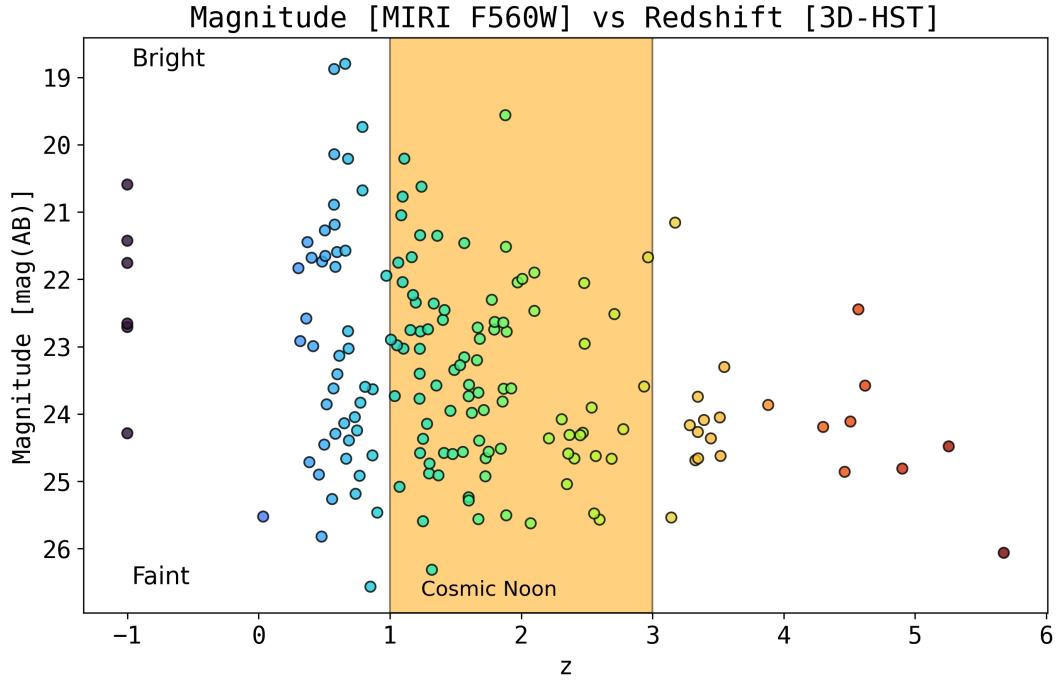


Figure 7: Scatter plot of Magnitudes vs Redshift showing the redshift distribution of the detected sources with respect to their magnitude. The orange band marks the area of $z \sim 1-3$

sizes of the detected sources by comparing their Kron Radius in the fig. 8. Although we can't only rely on this and therefore, the study demands a more robust comparison by estimating the Sérsic radius of the detected sources and

comparing them. Publicly available morphological measurements for galaxies in the HST imaging from the CANDELS fields have been performed by [Madau and Dickinson \(2014\)](#), but these do not include the results for the AEGIS

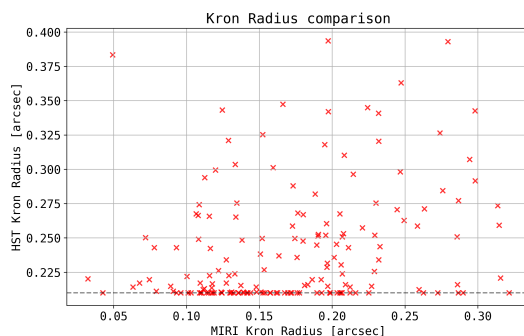


Figure 8: Comparison plot of Kron Radius of detected sources as reported in the 3D-HST catalog.

field. Redoing the size measurements from the HST imaging was beyond the scope of this project.

Fig. 9 showcases that the majority of the analysed galaxies have a half-light radius of less than 1" majorly following the low Sérsic Index too. There are a few outliers with half-light radius greater than 2" which, together with eyeballing, signifies that for a few galaxies, the fitter stuck at a local minimum, therefore, resulting in absurd values. These galaxies can be re-fitted with a compound Sérsic model in future for further analysis.

In fig. 10, we observed a significant offset between the calculated windowed coordinates of the detected sources and their reported values in the 3D-HST catalog. This offset is a curious result itself, as the MIRI6 image used for the analysis was astrometrically registered to HST/CANDELS v1.9 WFC3 and ACS images, as mentioned by Yang et. al 2022 (in prep).

Finally, in the CEERS MIRI6 pointing, we detected two sources that were not matched with the 3D-HST catalog at $1.6\mu m$ imaging, ex. fig. 11. This hints at one of the possible reasons that these might be the Lyman-break galaxies with the rest Lyman-limit at $0.912\mu m$ and must have $z > 0.8$ in order to go undetected in $1.6\mu m$ imaging. As these two sources were also present in the F770W imaging, this gives a strong statement of these sources being high-redshift Lyman-break galaxies.

VI. FUTURE PROSPECTS

This study can further proceed towards estimating the exact morphological parameters of the detected galaxies and successfully integrating that process into the main pipeline. Once done, one can look deeper by plotting photometric SEDs of the detected sources.

ACKNOWLEDGMENTS

This work was performed as part of the HiWi project done at Dr. Fabian Walter's group at the Max Planck Institute for Astronomy, Heidelberg, under the supervision of Dr. Leindert Boogaard.

I want to thank Leindert for his constant support and guidance and for being patient with my doubts and breaks during the whole project. His enthusiasm for the field of Galaxy Evolution served as a big inspiration for pushing myself carefully and strongly. I would also like to thank Fabian for his support and for allowing me to join his group in the first place.

I would also like to thank my colleague, Simran Joharle, for teaching me the basics of Source-Extractor and Photometry, which helped me to speed up the progress of the project by quite a lot and for being a wonderful and supportive study partner during the whole semester.

Last but not least, I would like to thank this beautiful city of Heidelberg for inspiring me every day to explore and solve the mysteries of nature and for taking away my stress with its beautiful sunsets.

VII. APPENDIX

A. Code for creating Erosion Mask for MAST files

```
# making the boolean mask
mask = hdu[1].data # defining the mask
mask[np.where(mask!=0)] = 1 # setting
→ non-zero values to 1
```

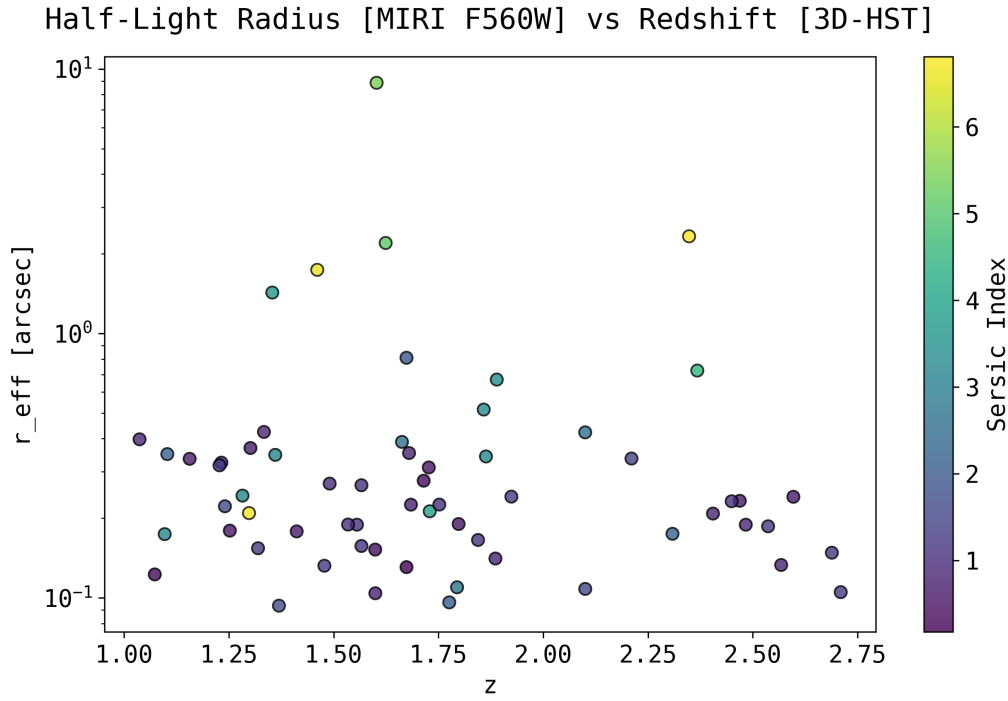


Figure 9: Scatter plot of the half-light radius vs redshift of the galaxies at cosmic noon. The colormap in the plot stands for the Sérsic index of the galaxies.

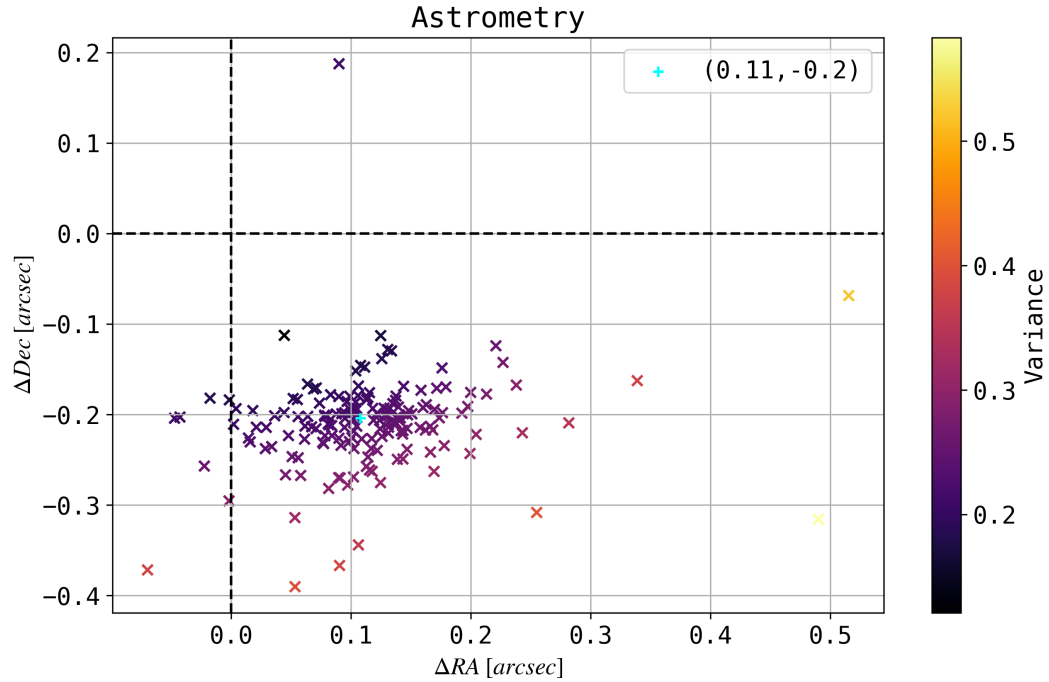


Figure 10: Plot of the astrometric difference between the coordinates of the detected sources and their reported coordinates in the 3d-HST catalog.

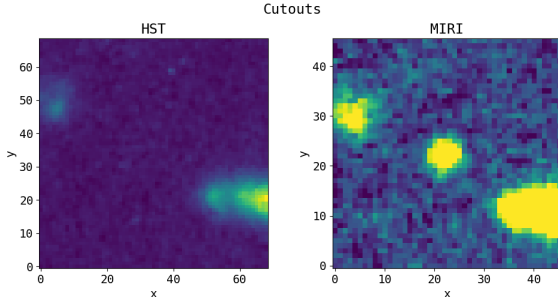


Figure 11: Cutout of the undetected source in the 3D-HST mosaic of AEGIS field in F160W and the MIRI mosaic of pointing 6 in F560W.

```

4 mask[930:995,152:154] = 0    # hacking
   ↵ extra rows for better masking in the
   ↵ coronograph FOV
5
6 # eroding the edges of the mask
7 mask_ero = binary_erosion(mask)
8 for i in range(13):
9     mask_ero = binary_erosion(mask_ero)

```

B. Code snippet for generating a table of the extracted sources on CEERS MIRI DR0.5 fits files.

```

# importing the custom functions
from scripts.jwst_func_red import
   ↵ jwst_cataloger
from scripts.sep_conv_masks import
   ↵ Conv_Masks
import numpy as np
import pandas as pd

# defining the parameters to input in
   ↵ SEP
sep_params = {'thresh':0.9, 'minarea':3,
   ↵ 'deblend_nthresh':64,
   ↵ 'deblend_cont':0.0008,
   ↵ 'clean_param':1.0,
   ↵ 'filter_kernel':Conv_Masks().gauss_4_7x7()}

```

```

'filter_type':'conv',
'kron_params':[3,(0.207/0.09)/2]}

# getting the output tables
source_table, crossmatch_table,
   ↵ catalog_table, data, rms, header,
   ↵ seg =
   ↵ jwst_cataloger("~/miri6_f560w_dr0.5_i2d.fits",
'~/aegis_3dhst.v4.1.cat.FITS',
ref_cat_file_type = "fits",
hdu_info = False, data_contgplots =
   ↵ True,
binary_ero = False, phy_unit='MJy/sr',
flux_rad_conv = True, **sep_params)

```

The `jwst_cataloger` function returns:

- `sourceTable`: `astropy.table.Table`, Table containing all the properties of detected objects
- `matched_sources`: `astropy.table.Table`, Table containing only those objects which are matched with ref catalog
- `ref_sources`: `astropy.table.Table`, Table containing the matched sources from the reference catalog (only if `ref_catalog` is provided)
- `data`: `numpy.ndarray`, The data array
- `rms`: `numpy.ndarray`, The rms array
- `header`: `astropy.io.fits.header.Header`, The header of the data
- `seg`: `numpy.ndarray`, The segmentation map

and plots the detected, catalog, and cross-matched sources.

The complete notebook for extraction and morphology fit can be found on the GitHub repository.

C. PetroFit plots at different redshifts

Below are the plots on the morphological fitting of a few galaxies at the cosmic noon. The sample is chosen at varying redshifts and shapes

to show the robustness of the fitting pipeline using **PetroFit**. The last three plots also showcase the spirals identified after Sérsic fitting.

- K. Barbary, Journal of Open Source Software **1** (6), 58 (2016). [2](#)
- E. Bertin and S. Arnouts, Astron. and Astrophys. Suppl. **117**, 393 (1996). [2](#)
- G. B. Brammer, P. G. van Dokkum, M. Franx, et al., Astrophys. J. Suppl. **200** (2), 13 (2012). [2](#)
- S. L. Finkelstein, M. B. Bagley, P. A. Haro, et al., Astrophys. J. **940** (2), L55 (2022). [2](#)
- S. L. Finkelstein, M. Dickinson, H. C. Ferguson, et al., The Cosmic Evolution Early Release Science (CEERS) Survey, JWST Proposal ID 1345. Cycle 0 Early Release Science (2017). [2](#)
- A. Galametz, A. Grazian, A. Fontana, et al., Astrophys. J. Suppl. **206** (2), 10 (2013). [2](#)
- R. Geda, S. M. Crawford, L. Hunt, et al., The Astronomical Journal **163** (5), 202 (2022). [7](#)
- J. S. Kartaltepe, C. Rose, B. N. Vanderhoof, et al., Astrophys. J. **946** (1), L15 (2023). [2](#)
- P. Madau and M. Dickinson, Annual Rev. Astron. Astrophys. **52**, 415 (2014). [1, 9](#)
- I. G. Momcheva, G. B. Brammer, P. G. van Dokkum, et al., Astrophys. J. Suppl. **225** (2), 27 (2016). [2](#)
- R. E. Skelton, K. E. Whitaker, I. G. Momcheva, et al., Astrophys. J. Suppl. **214** (2), 24 (2014). [2](#)
- K. A. Suess, R. Bezanson, E. J. Nelson, et al., Astrophys. J. **937** (2), L33 (2022). [2](#)
- A. van der Wel, M. Franx, P. G. van Dokkum, et al., Astrophys. J. **788** (1), 28 (2014). [1](#)

